Letter

# Enhancement of superconductivity upon reduction of carrier density in proximitized graphene

Gopi Nath Daptary, Udit Khanna, Eyal Walach, Arnab Roy, Efrat Shimshoni, and Aviad Frydman
*Department of Physics, Jack and Pearl Resnick Institute and the Institute of Nanotechnology and Advanced Materials, Bar-Ilan University, Ramat-Gan 52900, Israel*

(Received 20 October 2021; accepted 7 March 2022; published 25 March 2022)

The superconducting transition temperature ($T_c$) of single-layer graphene coupled to an indium oxide (InO) film, a low carrier-density superconductor, is found to increase with *decreasing* carrier density and is largest close to the average charge neutrality point in graphene. Such an effect is very surprising in conventional BCS superconductors. We study this phenomenon both experimentally and theoretically. Our analysis suggests that the InO film induces random electron and hole doped puddles in the graphene. The Josephson effect across these regions of opposite polarity enhances the Josephson coupling between the superconducting clusters in InO, along with the overall $T_c$ of the bilayer heterostructure. This enhancement is most effective when the chemical potential of the system is tuned between the charge neutrality points of the electron and hole doped regions.

DOI: 10.1103/PhysRevB.105.L100507

Low carrier-density superconductivity has been a topic of great interest in condensed matter research since its discovery in $SrTiO_3$ [1]. In conventional BCS superconductors, the critical temperature $T_c$ is known to increase with increasing carrier density ($n$) [2]. Contrarily, experiments on a number of exotic low-density superconductors, such as Li-intercalated layered nitrides [3,4], underdoped $La_{2-x}Sr_xCuO_4$ [5], etc., detected an enhancement of $T_c$ with decreasing $n$. These results were interpreted as evidence for a non-BCS mechanism of electronic pairing, such as electron-electron (rather than electron-phonon) interactions [6,7]. To date a mechanism for the enhancement of $T_c$ upon reducing $n$ for a BCS superconductor is lacking. In this Letter, we present results of a conventional superconducting system in which $T_c$ is largest close to a charge neutrality point (CNP) for which $n$ can be extremely small.

Two-dimensional superconductors, in which the chemical potential can be modulated by the gate voltage ($V_g$), are an ideal system for approaching the ultralow carrier-density regime. Graphene [8] is unique in this sense since the low-energy dispersion is linear with momentum, i.e., the conduction and valence band touch at discrete points (Dirac points) resulting in a gapless semiconductor [9]. Hence $n$ can be tuned through the CNP and may, in principle, be as small as desired. In this Letter we show that coupling graphene to a highly disordered, low-density superconductor gives rise to a unique situation as the superconducting islands induce hole-doped regions within graphene, thus generating two CNPs (discussed later) in place of the global Dirac point for nonproximitized graphene. This leads to a unique situation where superconductivity is enhanced with decreasing $n$ and is strongest close to the average CNP. We present a model to explain this extraordinary result based on the Josephson effect between regions of opposite polarity within the graphene. We show that the Josephson coupling between different superconducting regions is maximal when the system is tuned approximately halfway between the charge neutrality points of the electron and hole doped regions. This occurs close to the global CNP of the graphene layer in the heterostructure.

The experiments were performed on heterostructures of single-layer graphene (SLG) and thin amorphous indium oxide (InO). We use chemical vapor deposition (CVD) grown SLG sheets transferred onto 285 nm $SiO_2$ on top of a Si wafer as a two-dimensional (2D) material. The sample was patterned into a Hall bar geometry by standard e-beam lithography and contacted to Cr/Au leads (5 nm/30 nm). It was then covered by a 30-nm-thick InO film via a second lithography step. For reference, we prepared similar geometries of bare graphene and bare InO [see Fig. 1(a)]. The channel length and width of the sample are 150 and 50 $\mu$m, respectively. The carrier density of the graphene device was modulated by changing the gate voltage applied to the back side of the Si wafer. The device structure along with the electrical connections are shown in Fig. 1(a). Measurements were performed in a wet He-3 system at temperatures down to 0.3 K.

InO is a low-density superconductor where $n$ can be controlled between $\sim 10^{19}$ and $10^{20}$ cm$^{-3}$ by changing the $O_2$ partial pressure during film deposition [10]. For large $n$, the critical temperature $T_c$ can reach $\sim$3.5 K and the coherence length $\xi$ is 30–50 nm [11,12]. Decreasing $n$ causes the InO film to undergo a transition from a superconducting state to an insulating state. Nevertheless it has been shown that in both phases, the film includes emergent superconducting puddles, with sizes of a few $\mu$m, embedded in an insulating matrix [13–15]. Indeed, a comparable finite energy gap $\Delta$ and vortex motion were measured in both phases [12,16–20]. The difference between a superconducting film and an insulating one lies in the global superfluid density which depends on the Josephson coupling between superconducting puddles [21]. This is illustrated schematically in Figs. 1(b) and 1(c) which show the resistance versus temperature curves of two InO films: one insulating, denoted as sample I [Fig. 1(b)], and one superconducting, denoted as sample S [Fig. 1(c)], together with sketches of the inherent superconducting granularity. In

 

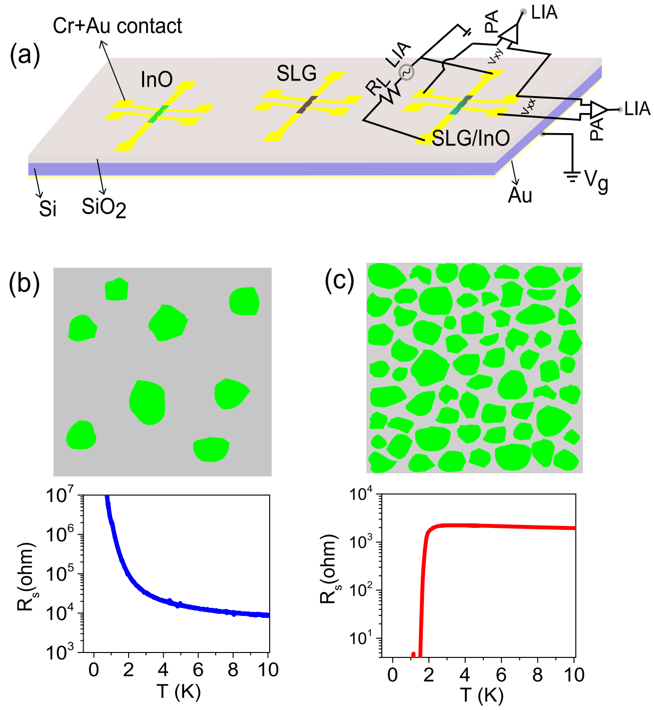


FIG. 1. (a) A schematic diagram of the devices (from left: InO, SLG, and an InO/SLG heterostructure). The longitudinal and transverse voltages are measured by a lock-in amplifier (SR 830) after amplification of the signals by a low-noise preamplifier (PA-SR552). The carrier density is modulated by the back-gate voltage $V_g$ applied to the contact at the bottom of the Si. (b) and (c) Sketches of the superconducting islands and the resistance vs temperature curves of samples I and S, respectively.

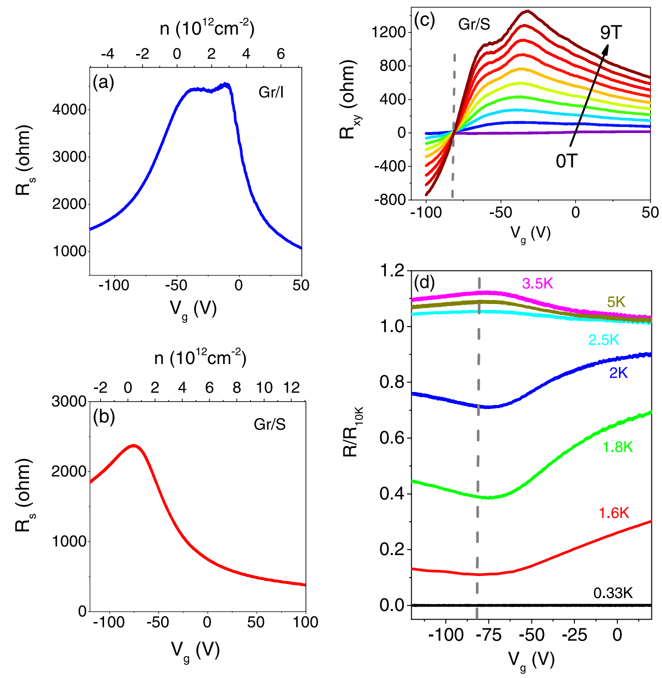


FIG. 2. (a) and (b) Sheet resistance $R_s$ as a function of $V_g$ of sample Gr/I and sample Gr/S, respectively, at zero magnetic field. The measurements were performed at $T = 1.7$ K for Gr/I and at $T = 5$ K ($T > T_c$) for Gr/S. (c) Hall resistance $R_{xy}$ as a function of $V_g$ at different magnetic fields ($B = 0$–$9$ T in steps of 1 T) at $T = 1.7$ K of sample Gr/S. Note that the charge neutrality point is at a gate voltage of $V_d = -81.5$ V. (d) Sheet resistance, normalized by the resistance at 10 K, as a function of $V_g$ at different $T$ of sample Gr/S. The slight difference between the CNP extracted from the Hall measurement and that of the resistance peak is attributed to the disorder of the sample which leads to some spatial distribution of $n$. Note that the resistance reaches a maximum at $T = 3.5$ K. This is due to the nonmonotonic nature of the indium oxide film transport [20].

the insulating phase the superconducting islands are sparse and decoupled, so that superconductivity is present only locally, while in the superconducting phase Josephson coupling percolates across the sample and global superconductivity is achieved. In this Letter we discuss the results from two of the samples, Gr/S and Gr/I, which are heterostructures of SLG and a thin InO layer in the superconducting or insulating phase, respectively. A second superconducting sample (Gr/S2) showed similar results as shown in the Supplemental Material (SM) [22]. In a previous work we presented the results on sample Gr/I [24]. In such a system the rather sparse InO superconducting puddles proximitize the underlying regions in the graphene sheet, at the same time hole doping them relative to the remaining SLG. Hence, the system includes a second charge neutrality point in addition to the usual CNP of the overall electron-doped graphene ($DP_e$) [24]. This point, dubbed the "hole Dirac point" ($DP_h$), gives rise to an additional peak in the resistance versus gate voltage ($R$-$V_g$) curve as seen in Fig. 2(a). Unlike most experiments of SLG coupled to a BCS superconductor, the low carrier density of InO (a few orders of magnitude smaller than conventional superconductors) makes it experimentally possible to access both CNPs, i.e., $DP_e$ and $DP_h$ in sample Gr/I. Our results also indicate that in samples for which the InO film is closer to the superconducting transition, the separation (in energy) between $DP_e$ and $DP_h$ is larger [24], thus making it experimentally difficult to probe both CNPs. Nevertheless, a large region around the midpoint between $DP_e$ and $DP_h$ is accessible.

In the current work, we focus on Gr/S. Figure 2(b) shows that for high temperatures $T$ significantly above $T_c$, one resistance peak is observed. Hall effect measurements [see Fig. 2(c)] identify this resistance peak as the charge neutrality point of the system. Surprisingly, as the temperature is lowered close and below $T_c$, the peak at the CNP turns into a dip which becomes sharper with decreasing $T$, until a sufficiently low temperature at which the sample becomes superconducting in the entire $V_g$ regime [see Fig. 2(d)]. This dip implies that superconductivity is *strongest* close to the CNP.

This notion is further supported by the $R(T)$ curves at different $V_g$ presented in Fig. 3 for sample Gr/S. For all gate voltages the heterostructure shows superconductivity at low temperatures. However, it is seen that $T_c$ (defined as the temperature at which the resistance drops to 90% of the normal sheet resistance at 10 K) systematically increases as $n$ decreases and reaches a maximum around the high-temperature CNP. This is in stark contrast with the common behavior of conventional superconductors and with previous experiments

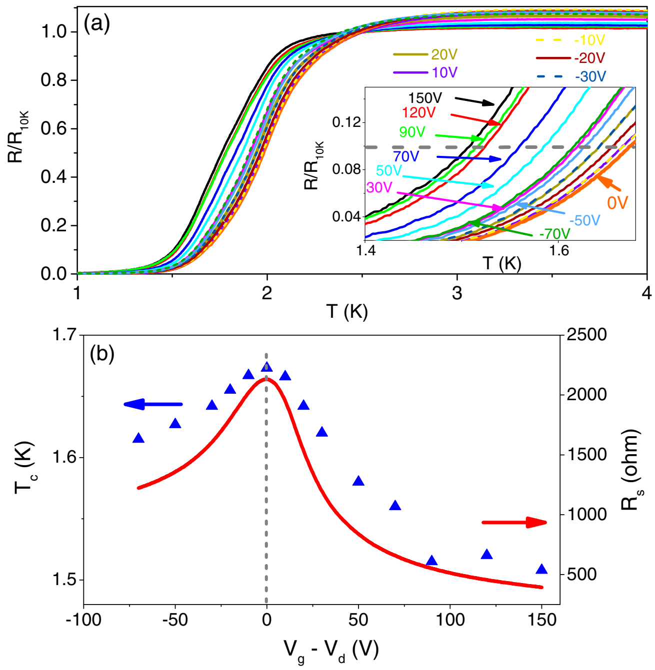


FIG. 3. (a) Sheet resistance $R_s$ normalized by the resistance at 10 K, as a function of temperature at different gate voltages relative to the CNP, $V_g - V_d$, of sample Gr/S. Inset: A zoom on the small temperature range highlighting the evaluation of $T_c$ with gate voltage. (b) $T_c$ and $R_s$ at $T = 5$ K as a function of $V_g - V_d$ measured at $B = 0$ T.

of Sn dots on graphene [25] which exhibit a minimum of $T_c$ at the CNP.

A possible explanation for such behavior would be to invoke a non-BCS pairing mechanism in the proximitized islands in graphene. Such mechanisms have been used to explain the enhancement of superconductivity of exotic low-density superconductors [7,26,27]. However, there seems to be no reason to assume that superconductivity in InO is of an unconventional nature and hence any superconducting regions in the proximitized graphene are unlikely to show non-BCS properties. Instead, we suggest that in our samples, the graphene provides a medium for Josephson coupling between the superconducting clusters of InO, thereby enhancing the superfluid stiffness. We emphasize that, just as in the bare InO thin films, $T_c$ is dictated by the stiffness which controls phase fluctuations among the superconducting clusters, and not by the pairing amplitude. In the Gr/S heterostructure, it is maximally close to the average CNP because (as shown below) the Josephson effect through puddles of opposite polarity in the graphene layer is strongest when their average density is close to zero.

In clear contrast to sample Gr/I, in sample Gr/S the volume fraction of superconducting islands within the InO is roughly equal to that of the insulating regions [see Fig. 1(c)]. In the underlying SLG, this generates large hole-doped puddles with proximity-induced superconductivity embedded in an electron-doped background. These superconducting islands are absent at temperatures far above $T_c$ since no emergent granularity is expected in the normal state [15] of InO. In this case, both electron-doped and hole-doped regions in the SLG contribute equally to the transport. Thus, Hall measurements feature a CNP (consistent with the observation of a peak in the (longitudinal) resistance as a function of the gate voltage [Fig. 2(d)] for $T$ larger than 2.5 K) when the average density of the sample is zero, i.e., the electron and hole densities are roughly equal. However, as $T$ is reduced and transport flows mostly through the superconducting islands, the finite resistance is dominated by patches of the SLG underlying the narrow constrictions between them. These effectively become SNS junctions where the S regions are hole doped compared to the N region.

The proper model for the system at low $T$ is therefore a random array of Josephson junctions, where the Josephson coupling (ultimately dictating $T_c$ of the network) is provided by SNS constrictions of varying sizes. To analyze their $V_g$ dependence, we consider a single SNS weak link and calculate its critical current ($I_c$) at $T = 0$ (see SM for details [22]). The Fermi energy in the normal (N) region ($E_F$) is assumed to be positive, while the Fermi energy in the superconducting (S) regions ($E'_F = E_F - U$) is negative. The difference between the two ($U$) is assumed to arise from the difference in the electrostatic potential induced by the superconducting puddles in the InO. When $V_g$ is varied, $E_F$ and $E'_F$ shift while maintaining $U$ fixed. The Josephson coupling of the junction is proportional to its critical current $I_c$. The length ($L$) of the weak link is assumed to be much smaller than the superconducting coherence length ($\xi$). In this limit, the contribution to the supercurrent from the continuum states may be neglected, and only the contribution from the subgap ($\epsilon < \Delta$) Andreev bound states needs to be computed [28,29]. We also assume $L \ll W$ (the width of the link) so that there is a single bound state for each transverse wave vector.

Graphene SNS junctions have been studied previously in great detail [30–33], including in the limit considered here [30]. However, the previous works only considered the case where superconducting regions were heavily doped compared to the normal region. These studies find that $I_c$ is minimal at the Dirac point of the normal region and increases monotonically as the carrier density $n$ is increased. This behavior is compatible with, e.g., the experiments based on granular Sn islands deposited on a single layer of graphene [25], where the S regions are metallic superconductors.

Our model goes beyond previous works in that we relax the assumption of very heavily doped superconducting regions. Furthermore, in our case the unique scenario dictated by the experimental system forces us to explore the regime where the carrier densities in the superconductor and normal regions are close to each other in magnitude, but opposite in sign. We evaluate the spectrum of the subgap Andreev bound states $\epsilon_q^{\mathrm{ABS}}$ in such a Josephson junction as a function of the phase difference between the superconducting regions ($\phi$). The equilibrium Josephson current may be found through

$$I(\phi) = -4\frac{e}{\hbar}\sum_q \frac{\partial \epsilon_q^{\mathrm{ABS}}}{\partial \phi}. \qquad (1)$$

Here, the factor of 4 accounts for the spin and valley degeneracies. The critical current $I_c$ is simply the maximal value of $I(\phi)$. As explained earlier, the behavior of $I_c$ as a function of

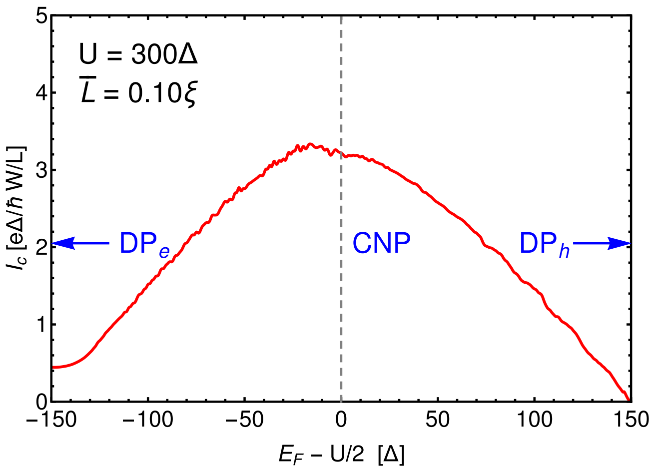


FIG. 4. The critical current ($I_c$) as a function of the Fermi energy relative to the CNP (in units of $\Delta$). The leftmost (rightmost) energy corresponds to the DP$_e$ (DP$_h$). At the CNP, the carrier densities in the electron and hole regions are equal, so that the average density is zero. Contrary to the standard picture, $I_c$ is largest in the regime where the (net) carrier density is very small. This is a consequence of the opposite polarity of the superconducting and normal regions. The red curve shows $I_c$ after averaging over the length ($L$) of the SNS junction (keeping $\bar{L} = 0.1\xi$), in order to remove the length-dependent features and account for the disordered nature of the superconducting puddles. Here, the value of the electrostatic shift is $U = 300\Delta$.

the Fermi energy is expected to follow the variation of $T_c$ as a function of $V_g$ in the sample Gr/S.

Figure 4 shows the variation of the critical current as a function of the Fermi energy ($E_F$) in the normal region. Note that in our convention, DP$_e$ (DP$_h$) appears at $E_F = 0$ ($E'_F = E_F - U = 0$) which corresponds to the left (right) end of Fig. 4. The curve shown in Fig. 4 was obtained after averaging $I_c$ over several values of $L$ (length of the SNS junction). The averaging removes spurious oscillatory features which depend on the value of $L$ (see SM), leaving behind a prominent gross feature: a broad maximum in the doping dependence of $I_c$. This captures the situation in the experimental system, where the percolating network of superconducting islands is expected to be dominated by several, most resistive, hot spots (or Josephson junctions) of varying lengths.

When the Fermi energy is close to the DP$_e$ our results match those reported in Ref. [30], since the carrier density in the superconductors is quite large ($|E'_F| \gg E_F$). With increasing $E_F$, the average $I_c$ increases monotonically until $E_F \sim U/2$. At this point, the carrier density in the S and N regions is equal, and the average carrier density of the SLG is expected to be close to zero. Hence, we expect $E_F = U/2$ to be close to the global CNP in our heterostructure (sample Gr/S). Increasing $E_F$ beyond $U/2$ drives the system into another regime, where the carrier density of the normal region is larger than that of the superconductors. Andreev reflection at the two N-S interfaces is highly suppressed in this regime, leading to a rapid decrease in $I_c$ despite the increase of carrier density in the normal region. For this reason, we observe the largest Josephson effect near $E_F = U/2$. Since the average CNP in sample Gr/S was identified with this point, we expect to have the strongest Josephson coupling between the superconducting islands, and the largest enhancement in $T_c$, at the CNP. This is indeed consistent with our experimental observations (Fig. 3). Theoretically, $I_c$ has two local minima at the Dirac point of the normal region ($E_F = 0$) and that of the superconducting region ($E_F = U$). In our experiments, however, we were unable to reach the two Dirac nodes, and only observed that the $T_c$ keeps decreasing away from the CNP.

In summary, we have shown that coupling a SLG to a disordered, low-density superconductor leads to the result where superconductivity is strongest close to the average charge neutrality point of the graphene, in stark contrast to the situation in systems of SLG coupled to high-density superconductors. We ascribe this to the presence of regions of opposite charge polarity induced within the graphene which acts as a coupling medium for superconducting islands. This regime provides access to Andreev reflections in low-density S-N junctions, where the carrier density in the superconducting regions is possibly lower than the normal ones. Furthermore, in the presence of magnetic field, the interplay between superconductivity in such heterostructure and the quantum Hall effect can give rise to intriguing phenomena. These will be the subject of future studies.

We are grateful for help from I. Volotsenko, and useful discussions with J. Ruhman and N. Trivedi. G.N.D., A.R., and A.F. were supported by the Israel Science fund, ISF, Grant No. 1499/21 and the U.S.-Israel Binational Science Foundation (BSF) Grant No. 2020331. U.K., E.W., and E.S. were supported by Israel Science Foundations (ISF) Grant No. 993/19, and the U.S.-Israel Binational Science Foundation (BSF) Grants No. 2016130 and No. 2018726.

[1] J. F. Schooley, W. R. Hosler, and M. L. Cohen, Superconductivity in Semiconducting $SrTiO_3$, Phys. Rev. Lett. **12**, 474 (1964).

[2] M. Tinkham, *Introduction to Superconductivity* (Courier Corporation, North Chelmsford, MA, 2004).

[3] Y. Taguchi, A. Kitora, and Y. Iwasa, Increase in $T_c$ upon Reduction of Doping in $Li_xZrNCl$ Superconductors, Phys. Rev. Lett. **97**, 107001 (2006).

[4] Y. Nakagawa, Y. Saito, T. Nojima, K. Inumaru, S. Yamanaka, Y. Kasahara, and Y. Iwasa, Gate-controlled low carrier density superconductors: Toward the two-dimensional BCS-BEC crossover, Phys. Rev. B **98**, 064512 (2018).

[5] O. Yuli, I. Asulin, O. Millo, D. Orgad, L. Iomin, and G. Koren, Enhancement of the Superconducting Transition Temperature of $La_{2-x}Sr_xCuO_4$ Bilayers: Role of Pairing and Phase stiffness, Phys. Rev. Lett. **101**, 057005 (2008).

[6] Y. Takada, *s*- and *p*-wave pairings in the dilute electron gas: Superconductivity mediated by the Coulomb hole in the vicinity of the Wigner-crystal phase, Phys. Rev. B **47**, 5202 (1993).

[7] M. Calandra, P. Zoccante, and F. Mauri, Universal Increase in the Superconducting Critical Temperature of Two-Dimensional Semiconductors at Low Doping by the Electron-Electron Interaction, Phys. Rev. Lett. **114**, 077001 (2015).

[8] A. K. Geim and K. S. Novoselov, The rise of graphene, Nat. Mater. **6**, 183 (2007).

[9] S. Das Sarma, S. Adam, E. H. Hwang, and E. Rossi, Electronic transport in two-dimensional graphene, Rev. Mod. Phys. **83**, 407 (2011).

[10] Z. Ovadyahu, Some finite temperature aspects of the anderson transition, J. Phys. C **19**, 5187 (1986).

[11] A. Johansson, G. Sambandamurthy, D. Shahar, N. Jacobson, and R. Tenne, Nanowire Acting as a Superconducting Quantum Interference Device, Phys. Rev. Lett. **95**, 116805 (2005).

[12] S. Poran, E. Shimshoni, and A. Frydman, Disorder-induced superconducting ratchet effect in nanowires, Phys. Rev. B **84**, 014529 (2011).

[13] D. Kowal and Z. Ovadyahu, Disorder induced granularity in an amorphous superconductor, Solid State Commun. **90**, 783 (1994).

[14] D. Kowal and Z. Ovadyahu, Scale dependent superconductor–insulator transition, Physica C: Supercond. **468**, 322 (2008).

[15] K. Bouadim, Y. L. Loh, M. Randeria, and N. Trivedi, Single-and two-particle energy gaps across the disorder-driven superconductor–insulator transition, Nat. Phys. **7**, 884 (2011).

[16] B. Sacépé, T. Dubouchet, C. Chapelier, M. Sanquer, M. Ovadia, D. Shahar, M. Feigel'man, and L. Ioffe, Localization of preformed Cooper pairs in disordered superconductors, Nat. Phys. **7**, 239 (2011).

[17] P. Spathis, H. Aubin, A. Pourret, and K. Behnia, Nernst effect in the phase-fluctuating superconductor $InO_x$, Europhys. Lett. **83**, 57005 (2008).

[18] D. Sherman, G. Kopnov, D. Shahar, and A. Frydman, Measurement of a Superconducting Energy Gap in a Homogeneously Amorphous Insulator, Phys. Rev. Lett. **108**, 177006 (2012).

[19] G. Kopnov, O. Cohen, M. Ovadia, K. H. Lee, C. C. Wong, and D. Shahar, Little-Parks Oscillations in an Insulator, Phys. Rev. Lett. **109**, 167002 (2012).

[20] A. Roy, E. Shimshoni, and A. Frydman, Quantum Criticality at the Superconductor-Insulator Transition Probed by the Nernst Effect, Phys. Rev. Lett. **121**, 047003 (2018).

[21] A. Kapitulnik, S. A. Kivelson, and B. Spivak, Colloquium: Anomalous metals: Failed superconductors, Rev. Mod. Phys. **91**, 011002 (2019).

[22] See Supplemental Material at http://link.aps.org/supplemental/10.1103/PhysRevB.105.L100507 for additional data on second device, optical image on the sample, detailed discussion on the theoretical calculation, which includes Ref. [23].

[23] Y. J. Shin, Y. Wang, H. Huang, G. Kalon, A. T. S. Wee, Z. Shen, C. S. Bhatia, and H. Yang, Langmuir **26**, 3798 (2010).

[24] G. N. Daptary, E. Walach, E. Shimshoni, and A. Frydman, Superconducting Dirac point in proximitized graphene, arXiv:2009.14603.

[25] A. Allain, Z. Han, and V. Bouchiat, Electrical control of the superconducting-to-insulating transition in graphene–metal hybrids, Nat. Mater. **11**, 590 (2012).

[26] L. Zhao, H. Deng, I. Korzhovska, M. Begliarbekov, Z. Chen, E. Andrade, E. Rosenthal, A. Pasupathy, V. Oganesyan, and L. Krusin-Elbaum, Nat. Commun. **6**, 8279 (2015).

[27] A. Di Bernardo, O. Millo, M. Barbone, H. Alpern, Y. Kalcheim, U. Sassi, A. K. Ott, D. De Fazio, D. Yoon, M. Amado, A. C. Ferrari, J. Linder, and J. W. A. Robinson, Nat. Commun. **8**, 14024 (2017).

[28] C. W. J. Beenakker and H. van Houten, Josephson Current through a Superconducting Quantum Point Contact Shorter than the Coherence Length, Phys. Rev. Lett. **66**, 3056 (1991).

[29] A. Furusaki, Josephson current carried by Andreev levels in superconducting quantum point contacts, Superlattices Microstruct. **25**, 809 (1999).

[30] M. Titov and C. W. J. Beenakker, Josephson effect in ballistic graphene, Phys. Rev. B **74**, 041401 (2006).

[31] A. M. Black-Schaffer and S. Doniach, Self-consistent solution for proximity effect and josephson current in ballistic graphene SNS Josephson junctions, Phys. Rev. B **78**, 024504 (2008).

[32] F. Mancarella, J. Fransson, and A. Balatsky, Josephson coupling between superconducting islands on single and bilayer graphene, Supercond. Sci. Technol. **29**, 054004 (2016).

[33] Y. Takane, Unified formula for stationary Josephson current in planar graphene junctions, J. Phys. Soc. Jpn. **89**, 094702 (2020).